Theoretical study of a laser with injected signal. I. Analytical results on the dynamics

H. Zeghlache and V. Zehnlé
Laboratoire de Spectroscopie Hertzienne, Université des Sciences et Techniques de Lille, Bâtiment P5, 59655 Villeneuve d'Ascq CEDEX, France
(Received 6 January 1992)

We have analyzed a model which describes a laser with an injected signal (LIS). We have used a simplified model, keeping only the complex-field equation. By means of standard mathematical methods, we have investigated the vicinity of a Hopf bifurcation point that it presents, and derived the normal form of the laser response. The parameter plane is fully analyzed in terms of the periodic-solution stability. A second branch of periodic solutions is also shown to be present in the system. Numerical simulations are carried out following the parameter-plane analysis and lead to the full set of bifurcation diagrams that this model can present. Finally, a global and complete view of the LIS dynamics is deduced.

PACS number(s): 42.65.−k

I. INTRODUCTION

The laser with injected signal (LIS), which is used experimentally to stabilize the output intensity or for mode selection, is also a well-known system investigated from the quantum-optic-instability point of view. The dynamics of externally injected lasers has been studied using very different assumptions for the parameter values. A larger number of studies based on several models, all derived from the Maxwell-Bloch (MB) formulation, have been performed to investigate the influence of different approximations and the effect of various parameters.

Most of the authors have kept the full homogeneously broadened atomic MB set: this represents a five-dimensional system with seven parameters. From the analytical point of view, the heaviness and the complexity of the expressions do not lead the way to any general treatment. The remaining track is either numerical simulations [1–7], which induces harsh restrictions on the results and reduces the global view of the parameter dependencies, or the adiabatic elimination of some variable [8–13] and the degenerate-case analyses based on very special parameter situations [14,15].

The numerical simulations reveal a large variety of self-pulsing behaviors and routes to chaos including quasiperiodicity and period doubling. Under high-gain conditions, regular and chaotic oscillations, envelope breathing, and spiking are shown to be present in such a formulation [1]. Analyses of power spectra, Poincaré maps, and Lyapunov exponents lead to detailed investigations of the bifurcation routes to chaotic attractors via subcritical or supercritical Hopf bifurcations of limit cycles, for example [2,3]. More generally, and even if one does not control globally the parameter space, the full set of equations has been studied in terms of identification of attractors, chaotic regimes, dimensionality, coexistence, and competition between different attractors. The complexity of such a system supplies the viewpoint of associated attractors, multiple competing attractors, and therefore structured chaos as shown by Jones and Bandy [7]. A generalized instability criterion, established for both optical bistability and LIS, has also been attempted by Hu Gang and Yang Guo-jian [6]: formal results have been derived and a global view versus the parameter space was obtained but via asymptotical studies.

The other way to study the MB equations occurs by adiabatically eliminating some variable (often the atomic polarization), and reducing the number of variables and parameters. Most of the publications on that subject are devoted to the case of CO_2 lasers (or class-B lasers) [8–13]. This leads to a three-dimensional problem and allows more global analytical studies. But in that case, the number of parameters (six) is still large and requires asymptotical analyses. Very special situations describing degenerate cases have been considered. They are characterized by a reduced number of parameters and then more sophisticated analysis can be proposed. This is the case of Politi, Oppo, and Badii [14], who have analyzed a degenerate Hopf bifurcation resulting from a coalescence of a Hopf bifurcation and a limit point of the steady states. This situation occurs for a suitable parameter range and is described by means of generic normal forms related to a degenerate codimension-2 phenomena. A frequency analysis was also performed [12]. Hu Gang and Yang Guo-jian [15] have shown that the five-dimensional system can be reduced to a two-dimensional set through adiabatic eliminations on a line of the space parameter where a codimension-3 bifurcation point is present. The vicinity of that critical point is then analyzed. On the same topic, the stabilizing effect of the detuning parameters has been analyzed on the three-dimensional LIS model by Braza and Erneux [13]: under some assumptions (small population inversion and adjusted detunings), it is shown that a subcritical Hopf bifurcation located on the intermediate branch, for small detunings, moves towards the upper-limit point (degenerate case) as the detunings are increased, and stable periodic solutions are then possible. It is a general feature of all these investigations on reduced LIS models that significant dynamical effects still persist in spite of a much smaller phase space.

Within the framework of reduced MB equations, some studies on NMR ruby laser with an injected signal, a

problem which is similar to the CO_2 LIS problem, have been performed experimentally first and then theoretically. A subcritical Hopf bifurcation has been observed and a three-dimensional model was proposed by Holzner *et al.* [16]. A normal form for a simplified two-dimensional model was derived and a general analysis was performed in the vicinity of the Hopf point but only for the experimental parameter values [17]. Braza and Erneux have carried out an asymptotic analysis of the periodic solutions of the NMR two-dimensional model as a function of the relative magnitude of the pump and injected amplitude parameters [18]. A complete branch of periodic solutions was described and the subcritical nature of the Hopf bifurcation was definitively demonstrated.

Only the field equation governs the description of class-A lasers such as the dye lasers. In Ref. [19], Spencer and Lamb provide the first-principles theoretical description of the LIS operation and derived the two-dimensional model, injecting a signal through a transmitting window of the laser cavity. They also went over a stability analysis. Some authors [12,13] have partially treated this two-dimensional model (in Appendixes) for comparison with the three-dimensional model results they have analyzed. Otherwise, numerical simulations on a modulated two-dimensional model have been performed by Yamada and Scholtz, leading to complex behaviors of the laser such as intermittency [20] and even chaos for the modulated-inversion layer system [21].

Most of these instability analyses have been carried out in the plane-wave approximation and infinite active medium in a ring cavity. Nevertheless, Lugiato *et al.* [29] have shown that a Gaussian transverse profile field may modify the results qualitatively and quantitatively: it increases the threshold level for injection locking relative to the plane-wave limit, and this induces a growth of the instability domain with respect to the injection strength. A bidirectional solid-state ring laser in the presence of two weak external signals (one in each direction) has been also modelized and experimentally investigated by Krivoshchekov *et al.* [22]. They have shown the stabilization of the output laser intensity and the suppression of the reverse wave when one input field is increased. A multimode laser with an injected signal has been considered by Bandy, Narducci, and Lugiato [3] showing a competition between the incident-field frequency and the mode-pulled frequencies of the modes that are present above the laser threshold.

These different kinds of analyses carried out on the LIS (and related systems) show the dispersion in the LIS dynamics research due to its complexity and different points of view. This explains the large number of behaviors one can find in the literature. However, the way the system undergoes the different stages and attains the complexity needs a more global description based on the parameter space analysis.

In order to explore the LIS behavior as a function of its parameters, and then to perform analytical calculations as far as possible, we choose to analyze the two-dimensional model. Our aim is to study what the remaining observations are that one could expect from such a simplified LIS description and make a link with previous works on higher-dimensional models. Curiously, no general and complete treatment has been performed yet on such a model.

This paper is organized as follows. In Sec. II we remind the MB formulation of the LIS, derive our simplified model, and describe briefly its steady states. The linear stability analysis is presented in Sec. III. The position of the instability point is fully discussed as a function of the parameters. In Sec. IV the vicinity of the Hopf point is analyzed using the normal form techniques to build the pulsating solutions which appear beyond the critical point. The stability of these periodic behaviors is derived. To present a complete bifurcation diagram, we cannot ignore a periodic branch of solutions rising at the lasing point characterized by the absence of the external field. Section V is devoted to some analytical calculations on that branch in accordance with those of Refs. [12,13]. Finally, numerical simulations supporting our previous analytical results are presented in Sec. VI. They give a global view on the dynamics of the model in the parameter space. A link will be made with previous analytical and numerical results obtained on a three-dimensional model.

II. THE FORMULATION

A. The model

The Maxwell-Bloch formulation for two-level atoms with an external driving field E_{ext} is the most common model describing a LIS. In standard notations, the equations are

$$\frac{dE}{d\tau}=-\kappa[E(1-i\nu)-E_{\text{ext}}]+igP \ , \tag{1a}$$

$$\frac{dP}{d\tau}=-\gamma_{\perp}(1-i\omega_a)P-igDE \ , \tag{1b}$$

$$\frac{dD}{d\tau}=-\gamma_{\parallel}(D-\sigma)-2ig(PE^*-EP^*) \ . \tag{1c}$$

The variables involved in this formulation are the complex laser field E, the atomic polarization P, and the population inversion D; κ, $\gamma_{\perp}$, and $\gamma_{\parallel}$ are the respective relaxation times, g is the coupling parameter between light and matter, ω_a and ν are the atomic and cavity frequencies, and E_{ext} is the external field [19]. The spatially-homogeneous-field approximation and single-mode operation are assumed for deriving the system (1). This model includes also a homogeneous broadening for the atomic subsystem.

When adiabatic elimination of both the atomic polarization and population inversion is valid, which is the Debye-laser's case for example, the Maxwell-Bloch equations can be reduced to a single equation for the complex field E [20,22]. A new time scale $t=\kappa\tau$ is then defined, and in terms of a complex rescaled variable X, the model becomes

$$\frac{dX}{dt}=-i\Omega X+\left[\frac{R}{1+XX^*}-1\right]X+\mathcal{A} \ , \tag{2}$$

where $E=\sqrt{\gamma_\perp\gamma_\parallel/4g^2}Xe^{i\Omega t}$, $E_{\text{ext}}=\sqrt{\gamma_\perp\gamma_\parallel/4g^2}\mathcal{A}e^{i\Omega t}$, and these equations express that X is given in a rotating frame related to the external injection: then any steady state corresponds in fact to a locked solution on the driving field. $R=\sigma g^2/\gamma_\perp$ is the usual pump parameter. The amplitude of the external field is $\mathcal{A}$. We note that the new variable and the parameters are dimensionless. In this paper, $\mathcal{A}$ is a constant parameter while in the following paper [23], we shall consider the case of a modulated input field.

We have supposed a zero-frequency detuning between the external field and the polarization on one hand, and the cavity on the other hand. Then in Eq. (2), the parameter Ω appears directly as the external-field frequency, but it can be easily replaced by (and even interpreted as) the frequency detuning between the driving field and the cavity. This is the case when $\Omega\neq\omega_a$ and $\Omega\neq\nu$ ($\omega_a\neq\nu$). One gets an identical evolution equation for the laser field, where the variable X and the parameter $\mathcal{A}$ are now rescaled by a constant value depending on the atomic–external-field frequency mismatch. From the dynamics point of view, no drastic modification of the system behavior can then occur.

The complex equation (2) is the simplest model describing a LIS. From a strictly mathematical point of view, we are left with a two-dimensional system governed by three parameters.

B. The steady states

The Cartesian form of the complex variable X is taken as $X=u+iv$. The steady states (u_S,v_S) are the zeros of the time derivative of the components u and v. One easily finds $u_S=-[R/(1+I_S)-1]I_S/\mathcal{A}$ and $v_S=-\Omega I_S/\mathcal{A}$, where $I_S=X_SX_S^*$ is the laser steady intensity and obeys the following implicit equation:

$$\left[\frac{R}{1+I_S}-1\right]^2 I_S+\Omega^2 I_S=\mathcal{A}^2=F(I_S)\ . \tag{3}$$

This last equation is a particular case of the more general steady solutions generated by the five-equation MB set and represents the possible locked intensities. A polar development of X leads also to the steady field phase given by the relation $\tan(\phi_S)=-\Omega\sqrt{I_S}/\sqrt{(\mathcal{A}^2-\Omega^2 I_S)^{1/2}}$: the steady states are phase-locked solutions. As a few parameters are involved, a parameter-diagram discussion on Eq. (3) is made much easier.

In the $(\mathcal{A},I)$ plane, the cubic Eq. (3) describes an S-shaped curve when the remaining couple of parameters (R,Ω) follows the inequalities:

$$\Omega^2<\frac{(R-1)^2(R+8)}{27R} \quad \text{and} \quad R>1\ . \tag{4}$$

$R=1$ is the usual laser threshold. The limit of the first inequality gives rise to the "bistable" line characterized by the presence of an inflection point on the steady curve: above that line, Eq. (3) has only one solution; the LIS presents a monostable behavior with respect to the signal strength $\mathcal{A}$. Otherwise, the steady curve shows three possible intensities for a fixed $\mathcal{A}$ parameter.

III. LINEAR STABILITY ANALYSIS

In order to test the stability of the steady state (u_S,v_S), we inject in Eq. (2) a perturbed solution of the form $u=u_S+\delta u e^{\lambda t}$ and $v=v_S+\delta v e^{\lambda t}$, where $\delta u\ll u_S$ and $\delta v\ll v_S$. At first order in $(\delta u,\delta v)$, one gets a linear problem with the following characteristic equation:

$$\lambda^2-2\lambda\left[\frac{R}{(1+I_s)^2}-1\right]+\frac{dF}{dI_S}=0\ . \tag{5}$$

The two roots of (5) are

$$\lambda_{1,2}=\frac{R}{(1+I_S)^2}-1\pm\left[\frac{R^2I_S^2}{(1+I_S)^4}-\Omega^2\right]^{1/2}\ . \tag{6}$$

Since no explicit form for I_S is available, direct analytical calculations cannot be carried out. However, one can get more information on the system behavior by treating partial results.

Depending on the values of the parameters, λ can be real or complex. A negative (positive) sign of its real part defines the stability (instability) of the steady state I_S. As a bifurcation parameter is varied, a sign change of the real part of a complex λ denotes the presence of a Hopf bifurcation and small amplitude oscillations of the intensity may settle in the system. While a real negative value of λ becoming real positive denotes a steady bifurcation, the system moves from a steady state to another if stable, or to some other attractor present in the phase space. [Note that with these elements and for optical bistability ($R<0$), an instability can never occur in such a system.] Back to the LIS, we can deduce the following:

(i) From Eq. (5) the negative-slope part of the S-shaped steady curve (or intermediate branch) is always unstable. The roots λ can never be complex on that branch: when it exists, the Hopf bifurcation is always on the upper or lower branch.

(ii) From Eq. (6) all steady intensities less than $\sqrt{R}-1$ are unstable.

(iii) The system presents a Hopf bifurcation when

$$\Omega^2>(\sqrt{R}-1)^2\ . \tag{7}$$

The limit of this last inequality gives the "Hopf line."

An exact calculation gives the position of the Hopf point on the S-shaped curve: it corresponds to an intersection between

$$I_H=\left[\frac{\mathcal{A}^2}{2}+\left[\frac{\Omega^6}{27}+\frac{\mathcal{A}^4}{4}\right]^{1/2}\right]^{1/3}+\left[\frac{\mathcal{A}^2}{2}-\left[\frac{\Omega^6}{27}+\frac{\mathcal{A}^4}{4}\right]^{1/2}\right]^{1/3} \tag{8}$$

and Eq. (3). The Hopf intensity is also characterized by the more useful relation

$$I_H=\sqrt{R}-1\ . \tag{9}$$

In the plane $(\mathcal{A},I)$ and then for a fixed value of R, the

Hopf point on the S-shaped steady curve occurs for a finite value of $\mathcal{A}$ given by the expression

$$\mathcal{A}_H=[I_H(I_H^2+\Omega^2)]^{1/2} . \tag{10}$$

At the critical point $X_H=u_H+iv_H$, the frequency Ω_H has the following form:

$$\Omega_H^2=\Omega^2-I_H^2=\Omega^2-(\sqrt{R}-1)^2=\frac{I_H^2}{u_H^2}(v_H^2-u_H^2) , \tag{11}$$

where the Cartesian coordinates of the complex electric field are

$$u_H=-I_H^2/\mathcal{A}_H \quad \text{and} \quad v_H=-\Omega I_H/\mathcal{A}_H . \tag{12}$$

One can note that the Hopf frequency is smaller than the external signal frequency: this represents globally a pulling frequency effect between $\mathcal{A}=0$ and $\mathcal{A}_H$. In this paper, HB stands for Hopf bifurcation.

Using the driving-field strength as a bifurcation parameter one can combine Eqs. (4) and (7) and define in the parameter space (R,Ω^2) three regions with different bifurcation diagrams. These regions are represented in Figs. 1(a) (for $R<4$) and 1(b) (for $R>4$) and Fig. 2 displays the diagrams occurring in each region. The three regions are

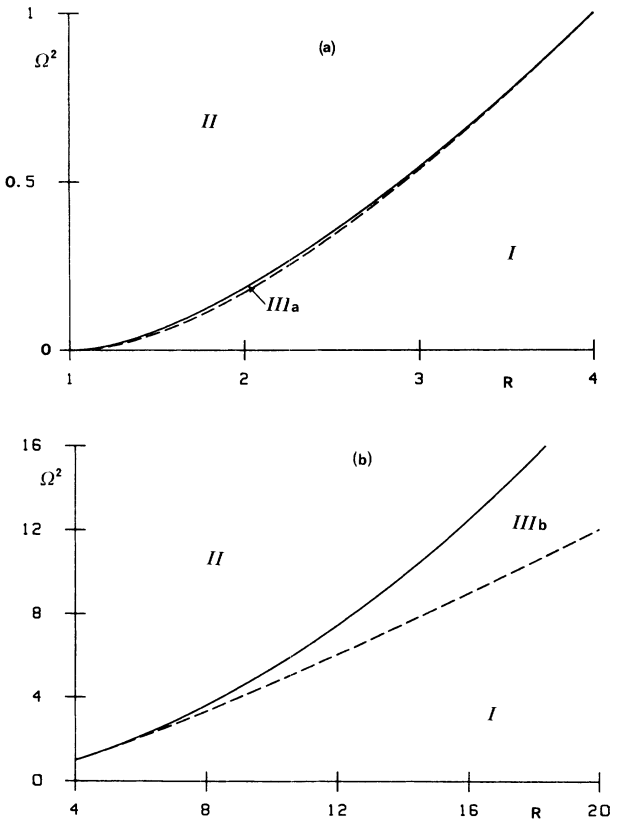

FIG. 1. Analysis of the parameter space (R,Ω^2). The dashed lines represent the equation: $\Omega^2=(\sqrt{R}-1)^2$ or the "Hopf line." The solid line stands for $\Omega^2=(R-1)^2(R+8)/(27R)$ or the "bistable line." Region I (III) presents bistability without (with) a HB. Region IIIa (IIIb) has a HB on the lower (upper) branch. Region II shows monostability with a HB (a) $R<4$, (b) $R>4$.

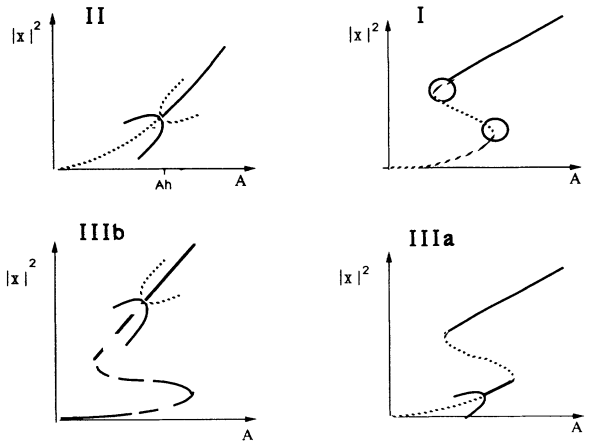

FIG. 2. All possible bifurcation diagram of system (2), depending on the parameter values. The dashed lines stand for unstable steady states while the solid line represents stable steady behaviors. The circles in region I represent the steady bifurcations at the turning points. The HB is represented by a two-pronged shape pitchfork and can destabilize the steady solutions stably or not (IIIa or IIIb).

delimited by the "bistable" and "Hopf lines." These two curves present an intersection point $(R=1,\Omega=0)$ and a tangency point $(R=4,\Omega=1)$: the "Hopf" line is always below the "bistable" line for $R>1$. According to these properties, the system can present the following bifurcation diagrams.

(i) Region I appears for small detunings Ω. No Hopf bifurcation can occur for these parameter values and the steady curve is always S shaped: the bifurcation points are steady and correspond to the turning points of the steady curve. Only the upper branch is stable since I_S must be larger than $\sqrt{R}-1$. As an example, one can consider the particular case of $\Omega=0$ and $R>1$ (and the lower boundary of region I) for which the destabilization occurs for $I_{c1}=R-1$ (the upper turning point). This is the usual lasing solution and corresponds to $\mathcal{A}=0$. The lower critical intensity is for $I_{c2}=-R/2-1\pm(R/2)\sqrt{1+8/R}$. This value is always smaller than $\sqrt{R}-1$. We can note that this last intensity value (which has no HB sense in this region) is embedded in the unstable intensity domain.

These results for $\Omega=0$, valid in the two-dimensional situation only, can be compared with those of Ref. [13] derived for the three-dimensional model and where numerical simulations show the presence of a HB point on the unstable intermediate branch. Globally, when we add the population inversion, and then a third parameter ($\gamma_\parallel$) to R and $\mathcal{A}$, the description in the parameter plane displays an increase of the Hopf existence domain involving the $\Omega=0$ line: the surface whose projection in the (R,Ω^2) plane is the Hopf line must reasonably curve itself towards low values of Ω and the Hopf existence domain can then hold the $\Omega=0$ line.

In the two-dimensional model the presence of the $\sqrt{R}-1$ intensity value on the intermediate branch occurs not only for $\Omega=0$ but also for all of region I. On the other boundary of region I given by Eq. (7), one can

find two bifurcation points: $I_{c1}=\sqrt{R}-1$ is the upper (lower) commutation point when $R>4(R<4)$. The second critical intensity occurs for

$$I_{c2}=-1-\frac{\sqrt{R}}{2}\pm\frac{\sqrt{R}}{2}\left[1+\frac{8\sqrt{R}}{R+2-2\sqrt{R}}\right]^{1/2}$$

and its position on the S-shaped curve is just at the second turning point.

(ii) In region II of the parameter space characterized by large values of Ω, the steady curve is monostable and the destabilization of I_S always occurs via a Hopf bifurcation. Particularly, on the bistable line, the HB occurs above the inflection point for $R>4$ and is present in some sense on the "upper" branch (or what will give the upper branch), while it appears below the inflection point for $R<4$ and thus on the "lower" branch (the intermediate branch is forbidden).

(iii) In between regions I and II, a third region takes place, noted as region III, for which a Hopf bifurcation occurs in a situation of a bistable steady behavior and still never on the intermediate branch. Two cases are possible depending on the location of the instability on the stable branches. Qualitative arguments indicate that this is related to whether R is smaller or larger than 4 as we will discuss now.

When Ω increases, the steady intensity decreases on the intensity axis: $dI_S/d\Omega$ is negative and inversely proportional to dF/dI_S. Thus the upper and lower branches come closer to the $\mathcal{A}$ axis. In the same way the steady solutions shift towards large values of $\mathcal{A}$, and the S-shape disappears progressively. Depending on the relative amplitude of the falling down motion of the steady branches and the position of I_H, one can conclude whether the Hopf point is climbing up or coming down on the upper or lower branch as we explain now. Since the upper branch has a large falling motion (dF/dI_s is large) and the Hopf intensity value is constant for a fixed R, one can deduce that the Hopf point has an ascendant behavior on that branch: this means that its distance to the upper turning point increases. This is the case for $R>4$ (or region IIIb).

When $R<4$, the HB is present on the lower branch of the S-shaped curve. Our analysis concludes to a decreasing motion of the instability point on that branch when Ω increases (region IIIa). These results do not contradict with conclusions obtained by continuity arguments between the upper and lower boundaries of region III. As suggested by Spencer and Lamb in Ref. [1] and demonstrated in this section, the presence of a Hopf bifurcation on the lower branch of the S-shaped steady curve occurs on a very narrow domain in the parameter space.

The two possibilities on whether the Hopf bifurcation is supercritical or subcritical are kept in Fig. 2 for regions II and IIIb. The stability of the periodic oscillations appearing beyond the Hopf critical point will be analyzed in the next section.

IV. CONSTRUCTION OF THE SMALL-AMPLITUDE PERIODIC SOLUTIONS

As the Hopf point is well defined, we focus on the solutions which may settle in the vicinity of that critical point. We shall try now an analytical and more precise description of them.

The standard perturbative method we use is developed in Ref. [24]. It consists of a study of the immediate neighborhood of the critical point and by constructing the analytic expression of the periodic solution of Eq. (2). We use again $\mathcal{A}$ as a bifurcation parameter, and consider the following expansion around the Hopf point:

$$\mathcal{A}=\mathcal{A}_H+\epsilon^2 a_2 \quad \text{with } \epsilon\ll 1 . \tag{13}$$

This defines a small parameter ϵ.

Since fast oscillations of our system are expected, a slow time scale τ (with respect to the rapid motion characterized by t) is also introduced, defined by

$$\tau=\epsilon^2 t \tag{14}$$

such that $d_t=\partial_t+\epsilon^2\partial_\tau$. The complex variable X is expanded as

$$X(t,\tau)=X_H+\epsilon X_1(t,\tau)+\epsilon^2 X_2(t,\tau)+O(\epsilon^3) \tag{15}$$

and reinjected in Eq. (2). The lowest order leads to the stationary condition at the Hopf point. At order ϵ one gets a linear problem, with two equations for u_1 and v_1, which can be written in vectorial form as

$$\partial_t X_1=\underline{L}X_1 , \tag{16}$$

where the $2\otimes 2$-matrix $\underline{L}$ is given in Appendix A, and whose solutions are given by

$$X_1(t,\tau)=\begin{bmatrix}u_1(t,\tau)\\ v_1(t,\tau)\end{bmatrix}=\begin{bmatrix}A(\tau)\\ B(\tau)\end{bmatrix}e^{i\Omega_H t}+\text{c.c.} \tag{17}$$

The coefficients A and B follow a slow time variation which has to be determined afterwards. They are related by

$$B(\tau)=\frac{u_H}{v_H}\left[-1+i\frac{\Omega_H}{v_H^2-u_H^2}\right]A(\tau)=QA(\tau) \tag{18}$$

and verify the so-called solvability condition

$$\partial_\tau A=(\alpha+i\beta)A+(\gamma+i\delta)A|A|^2 . \tag{19}$$

We do not present the tedious but straightforward calculations leading to the previous generic equation but for more details we give in Appendix A the broad outline of this mathematical method. Finally this solvability condition concerns the slow variation of the complex amplitude A of the periodic solution. In our case, the parameters of Eq. (19) have the following form:

$$\alpha+i\beta=\frac{4u_H a_2}{v_H^2-u_H^2}\left[\frac{1}{1+I_H}+i\frac{I_H(1-I_H)}{2\Omega_H(1+I_H)}\right] , \tag{20a}$$

$$\gamma=\frac{4I_H^2}{(v_H^2-u_H^2)^2}\frac{2v_H^2-1}{(1+I_H)^2} , \tag{20b}$$

$$\delta=-\frac{4}{3\Omega_H}\frac{I_H^2}{(v_H^2-u_H^2)^2}\times\left[6v_H^2-u_H^2-\frac{I_H}{1+I_H}(21v_H^2-u_H^2)+\frac{I_H^2}{(1+I_H)^2}(17v_H^2+3u_H^2)\right]. \quad (20c)$$

A straightforward study of Eq. (19) is realized. In polar coordinates $A=\rho e^{i\theta}$, the steady states are

$$\rho_S=0 \text{ and } \rho_S^2=-\alpha/\gamma \quad (21)$$

which need positive values. The finite small-amplitude periodic solution A_s occurs with a frequency $\omega_2=\beta+\delta\rho_s^2$. This value is proportional to a_2 and corresponds to a ϵ^2 correction to the Hopf frequency. Therefore X_1 oscillates with a frequency

$$\omega=\Omega_H+\epsilon^2\omega_2=\Omega_H+\epsilon^2\left[\beta-\delta\frac{\alpha}{\gamma}\right]. \quad (22)$$

A linear stability analysis of the steady solutions of Eq. (19) leads to a stability exchange between the zero- and finite-amplitude solution for $\alpha=0$, the zero solution being stable for $\alpha<0$. In our case, the small-amplitude oscillations beyond the Hopf point are stable (equivalently the Hopf bifurcation is supercritical) when $\alpha>0$ and $\gamma<0$. Since the expression of u_H is negative, one can find the condition $a_2<0$ and v_H^2 has to be less than $\frac{1}{2}$. This last inequality can also be written as

$$\Omega^2>\frac{(\sqrt{R}-1)^2}{2\sqrt{R}-3}. \quad (23)$$

All these results are summarized in Fig. 3 where we represent in the parameter space (R,Ω^2) the domains of existence and stability of the small-amplitude oscillations. We note the following: In the monostable region II, the Hopf bifurcation can be either supercritical or subcritical. In region III, the pulsating solutions are always stable when they appear on the lower branch (IIIa) and for $R>4$ (IIIb) the Hopf bifurcation is always subcritical. This explains the dashed or solid Hopf lines of Fig. 2 and their directions.

One can express the two conditions for a supercritical Hopf bifurcation as $\mathcal{A}<\mathcal{A}_H$ with $\mathcal{A}_H>\sqrt{2}\Omega(\sqrt{R}-1)$. In the bifurcation diagram $(\mathcal{A},I)$, the most eloquent inequality is $\mathcal{A}<\mathcal{A}_H$ (or $a_2<0$) while in the (R,I) plane the most useful relation is $v_H^2<(\frac{1}{2})$. From the frequency viewpoint, we can deduce from a study of Eq. (22) and the sign of ω_2, the evolution of the frequency of pulsating solutions in the surrounding of the bifurcation point and show that in general the ω_2 value is negative as $\mathcal{A}$ decreases from $\mathcal{A}_H$.

The calculations we have presented can be reproduced using R as a bifurcation parameter. One has to keep Eqs. (14) and (15), replace Eq. (13) by an expansion for R of the form $R=R_H+\epsilon^2R_2$, and follow the previous method. We get the same generic equation as Eq. (19), but the parameters α and β of Eq. (20) are modified as follows:

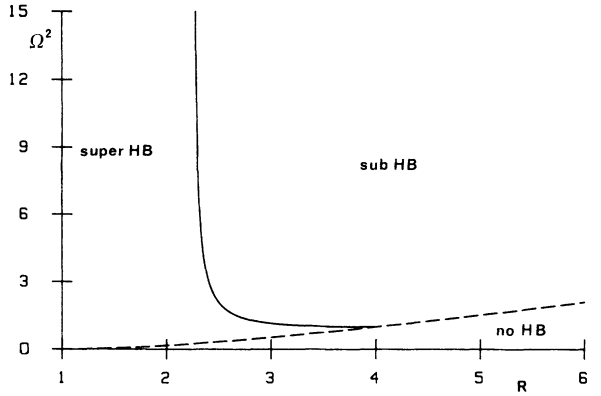

FIG. 3. Supercritical or subcritical HB: The dashed lines represent the function $\Omega^2=(\sqrt{R}-1)^2$ or the existence of the HB, and the solid line represents $\Omega^2=(\sqrt{R}-1)^2/(2\sqrt{R}-3)$, its stability (stable above).

$$\alpha'+i\beta'=\frac{R_2}{(v_H^2-u_H^2)(1+I_H)^2}\times\left[I_H+2u_H^2+i\frac{I_H(2u_H^2-I_H)}{\Omega_H}\right]. \quad (24)$$

The conclusions are qualitatively the same. The Hopf bifurcation is supercritical for $R_2>0$ and $v_H^2<\frac{1}{2}$. Note that the S-shaped steady intensity curve of the $(\mathcal{A},I)$ plane has a quite different shape in the (R,I) plane, and then when R is the bifurcation parameter.

V. THE SECOND BRANCH OF PERIODIC SOLUTIONS

The system (2) presents a second (and non-Hopf) branch of periodic solutions. This branch has been first described through its frequency view point by Oppo *et al.* [12] for the two- and three-dimensional LIS model using a Lindstedt-Poincaré expansion. In this section we develop a new calculation to characterize more precisely this limit cycle. When $\mathcal{A}=0$, one has to find the usual laser state whose intensity is $I=R-1$ and frequency Ω. For that reason, we follow this branch of solutions in the surrounding of $\mathcal{A}=a\epsilon$ ($\epsilon\ll1$). We take a, R, and Ω of order unity, and expand X as

$$X(t)=x_0+\epsilon x_1(t)+\epsilon^2x_2(t)+O(\epsilon^3). \quad (25)$$

After replacing X in Eq. (2), we get the first two orders

$$\frac{dx_0}{dt}=-i\Omega x_0+\left[\frac{R}{1+x_0x_0^*}-1\right]x_0, \quad (26a)$$

$$\frac{dx_1}{dt}=-i\Omega x_1+\left[\frac{R}{1+x_1x_1^*}-1\right]x_1+a-x_0\frac{R}{1+x_0x_0^*}\frac{x_0x_1^*+x_1x_0^*}{1+x_0x_0^*}. \quad (26b)$$

We present in Appendix B the direct integration of the system of Eqs. (26). The solution $X(t)$ of Eq. (2) can be then expressed at the two first orders as

$$X(t)=\sqrt{R-1}e^{-i\Omega t}+a\epsilon e^{-i\Omega t}\left[\frac{1}{k^2+\Omega^2}[k\cos(\Omega t)+\Omega\sin(\Omega t)]-i\frac{1}{\Omega}\cos(\Omega t)\right]+O(\epsilon^2)\ . \tag{27}$$

This form displays a time-dependent amplitude and phase corrections to the laser solution. Another way to express Eq. (27) is the following:

$$X(t)=\sqrt{R-1}e^{-i\Omega t}+a\epsilon\frac{k}{\Omega}\left[1-i\frac{k}{\Omega}\right]\frac{\cos(\Omega t)}{k^2+\Omega^2}e^{-i\Omega t}$$
$$-ia\epsilon\frac{\Omega}{k^2+\Omega^2}+O(\epsilon^2)\ . \tag{28}$$

It exhibits an order-ϵ constant shift on the v axis with respect to the Cartesian coordinates $x=u+iv$. Numerical simulations show also the presence of large limit cycles whose main feature is a center shift. This phenomena being persistent even for large values of the injection, it suggests a new analytic approach introducing this effect. We then seek a large-amplitude limit cycle existing even for large external injection. The presence of the center shift of the solutions can be injected in the following way:

$$X(t)=\begin{bmatrix}u(t)\\v(t)\end{bmatrix}=\begin{bmatrix}u_0\\v_0\end{bmatrix}+\rho(t)e^{i\psi(t)}\ . \tag{29}$$

We suppose u_0 and v_0 are constant, and for limit cycles the dominant orders of $\rho(t)$ can be supposed time independent. We inject Eq. (29) in Eq. (2) and after some modifications get the following equations:

$$\cos[\psi(t)]\{\mathcal{A}+\Omega v_0-u_0\}+\sin[\psi(t)]\{-\Omega u_0-v_0\}-\rho$$
$$+K(t)\{\rho+u_0\cos[\psi(t)]+v_0\sin[\psi(t)]\}=0\ , \tag{30a}$$

$$\cos[\psi(t)]\{-\Omega u_0-v_0\}+\sin[\psi(t)]\{-\mathcal{A}-\Omega v_0+u_0\}$$
$$-\Omega\rho+K(t)\{v_0\cos[\psi(t)]-u_0\sin[\psi(t)]\}$$
$$=\rho[d\psi(t)/dt]\ , \tag{30b}$$

where

$$K(t)=R/(1+u_0^2+v_0^2+\rho^2$$
$$+2\rho\{u_0\cos[\psi(t)]+v_0\sin[\psi(t)]\})\ .$$

No assumption concerning the other parameters has been emitted yet. However, one has to consider a small parameter, or more precisely a small parameter ratio, to simplify the $K(t)$ expression. We have tested several possibilities. The most conclusive situation is characterized by the following assumption: since we are interested in large-amplitude limit cycles, this supposes either large R or larger injections. In all cases, large values for ρ are expected and the couple (u_0,v_0) can be supposed much smaller than the ρ value. This situation is characterized by $1+\rho^2\gg u_0$ (or v_0) or even $\rho^2\gg u_0$ (or v_0) if $\rho^2\gg 1$. We are left with a situation which is similar to the one previously described for small injection, but more general in the sense that no smallness constraint on the external field amplitude is imposed. In fact, the equations impose $\mathcal{A}$ to be of order (u_0 or v_0), and since this couple of parameters can have reasonable values (but small with respect to ρ), this releases the small $\mathcal{A}$ assumption. We have found that a couple (u_0,v_0) may exist if

$$\rho^2\sim R-1+O(u_0^2,v_0^2,\ \text{or}\ u_0v_0)\ . \tag{31}$$

To be coherent with the large-ρ assumption we need large values for R. We can also derive the following expressions:

$$u_0=\mathcal{A}\frac{k}{k^2+\Omega^2}\ , \tag{32a}$$

$$v_0=-\mathcal{A}\frac{\Omega}{k^2+\Omega^2}\ . \tag{32b}$$

The shift on the v axis is identical to the one of Eq. (28) while a shift appears on the u axis. The phase at the dominant orders is also given by the expression

$$\psi(t)=-\Omega t-\frac{\mathcal{A}}{\Omega\sqrt{R-1}}\frac{k}{k^2+\Omega^2}$$
$$\times[-k\cos(\Omega t)+\Omega\sin(\Omega t)]\ . \tag{33}$$

These results look slightly different than the previous analyzed case. This is due to the different asymptotic limits we have considered: small $\mathcal{A}$ and reasonable values for Ω and R, or large values for $\mathcal{A}$ and R and still reasonable Ω. The conclusions one can deduce from these calculations are the following.

(i) For small injections, the center shift appears first on the v axis (while the injection acts normally on the u axis). As the injections are increased, the shift progressively leaves the v axis.

(ii) As we have imposed a constant amplitude to the limit cycle and the center shift, the phase has adjusted itself in a slightly different manner. We note that the phases in Eqs. (B6) and (33) do not have the same meaning and cannot be directly compared.

This phenomena is well known from the phase viewpoint [25,26]. The laser solution has a drift frequency due to the presence of one degree of freedom [27]. Then the periodic branch of solutions starting from the laser solution is characterized by an unbounded phase [13]. When the injection is added, the phase-locked steady solutions of the system are locked to the external frequency. As the injection is increased, the "laser" periodic branch develops itself and moves towards the locked solutions region. Its phase becomes progressively bounded (the phase drift is destroyed, the degree of freedom is lost), and this is realized via a center shift of the periodic solutions as we have shown in this calculation. The system chooses by itself an irreducible representation. The way this branch of periodic solutions develops needs a more

complete bifurcation diagram we shall present in the following numerical study.

VI. COMPLETE BIFURCATION DIAGRAMS

In this section we have computed the complete bifurcation diagrams for the output intensity. We have treated all the possible behaviors the two-dimensional system may exhibit when the input strength is varied. The previous analytical calculations have been helpful to scan carefully the (R,Ω) space. Moreover, as the system is only two dimensional, no "complicated" behavior, such as chaos or quasiperiodicity, is expected. In our case and since we have two kinds of periodic branches, one has to follow their evolution when the bifurcation parameter is varied. We have used AUTO [28] a computer software package that follows automatically the branches of periodic solutions using a continuation method. AUTO also determines the stability of the periodic solutions and locates a secondary bifurcation point if any. In all the bifurcation diagrams we present the dashed lines stand for unstable states while the solid line represents stable behaviors, the dark (white) circles are the L_2 norm of a stable (unstable) periodic solutions (complex output field), and the position of the HB is marked by a dark square. We shall present some numerical observations following the three regions already described in Sec. III.

(1) Region I is characterized by a missing Hopf bifurcation. We also know that the critical points are the upper and lower turning points, and the upper branch is always stable. In Fig. 4(a) we give the system behavior as a function of the input amplitude. The periodic branch, we call the "normal" lasing branch, has been computed starting from the lasing state for $\mathcal{A}=0$. The period of the solution is then $2\pi/\Omega$, and it increases along the branch very slowly first and then dramatically when the periodic solution approaches the steady-state branch near its upper turning point. The period of the pulsating solutions versus the input parameter is shown in Fig. 4(b). Note that the AUTO calculations are limited in the vicinity of the critical point (the turning point in this case): one has to take in account the computer precision. We have followed the periodic branch to 10^{-6} of the input-field value at the turning point and the period was evaluated to the 10^{+7}th order in dimensionless units. This reasonably allows us to conclude that the periodic branch and the steady curve merge at the upper turning point in an homoclinic orbit. The simulation we present has been realized for $R=2.0$ and $\Omega=0.2$.

No qualitative difference occurs when one of these two parameters is varied in region I. The junction between the periodic and steady lines always occurs on the upper commutation point. This description supports the system behavior for $\Omega=0$: the upper turning point and the lasing state for $\mathcal{A}=0$ coalesce in a homocline orbit (of period $2\pi/\Omega$).

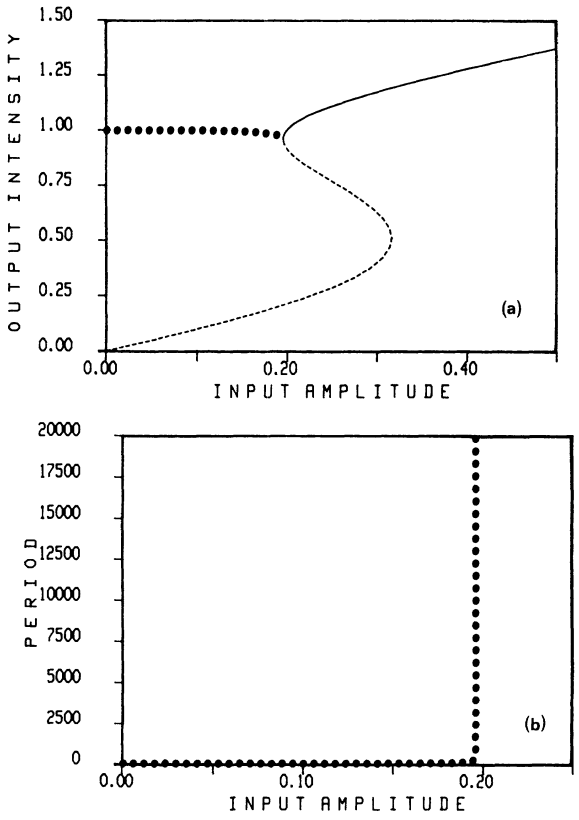

FIG. 4. Region I. (a) Typical bifurcation diagram for region I. The dark circles stand for the L_2 norm of the stable periodic solutions. (b) Related period of the pulsating branch.

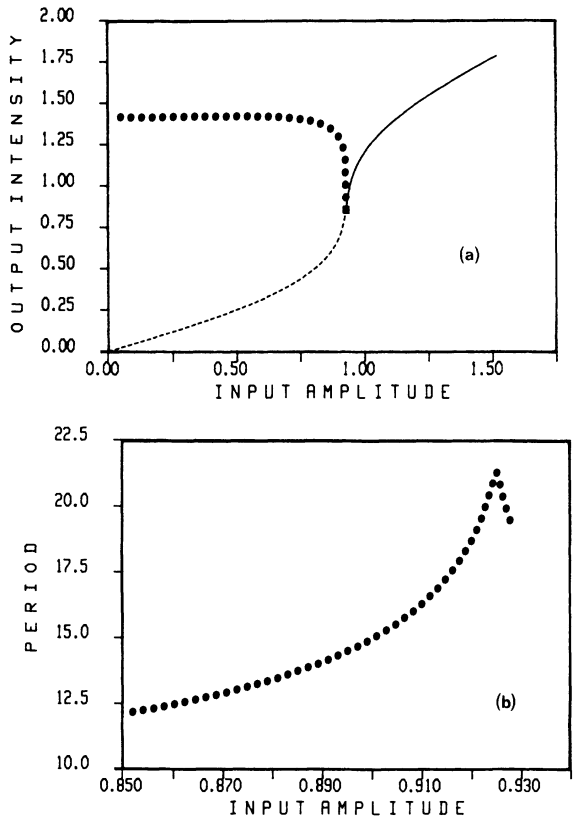

FIG. 5. Region II. (a) Bifurcation diagram with a supercritical HB. The square represents the Hopf bifurcation point and the dark circles represent the stable periodic branch. (b) Variation of the period versus the bifurcation parameter.

(2) Region II presents two kinds of bifurcation diagrams since the monostable steady curve can undergo either a subcritical or a supercritical Hopf bifurcation. The two cases are, respectively, displayed in Figs. 5 and 6. Above the Hopf bifurcation point, the steady solution is always stable. In case of supercritical Hopf bifurcation, the stable periodic branch appearing beyond the Hopf point (for $\mathcal{A} < \mathcal{A}_H$) directly merges in the normal branch [Fig. 5(a) for $R=3.0$, $\Omega=0.8$], its period increases to a maximum value then decreases to the lasing period $2\pi/\Omega$ [Fig. 5(b)]. Whereas in the subcritical case, the Hopf branch starts unstable in the "wrong" direction (or $\mathcal{A} > \mathcal{A}_H$), stabilizes at a "turning point," and then moves stably in the right direction (decreasing $\mathcal{A}$) towards the normal lasing branch [Fig. 6(a) for $R=5.0$, $\Omega=2.0$]. This trajectory makes possible a bistable behavior between steady and periodic stable solutions. In Fig. 6(b) one can follow the evolution of the period and note the only case for which the period decreases directly from the Hopf value to the external value.

(3) Region III is a quite narrow region in the parameter space, especially for reasonable values of R. The previous analytical results greatly serve the purpose of the numerical experiments: this is clearly expressed by the parameter values used to derive the diagrams. We uncover three types of bifurcation diagrams for this domain, one more than the two kinds we expected. They are shown in Figs. 7–9.

In region IIIb the system undergoes a subcritical Hopf bifurcation on the upper branch of the S-shaped steady curve. Figures 7(a) ($R=14.0$, $\Omega=3.0$) and its enlargement 7(b) do not contradict our previous conclusions. The trajectory of the periodic branch from the Hopf point to the lasing state (at $\mathcal{A}=0$) occurs in a very similar way in Fig. 6.

When R is less than 4, the Hopf bifurcation always appears supercritically on the lower branch (region IIIa) and Figs. 8(a) ($R=2.0$, $\Omega=0.425$) and 9(a) ($R=3.0$,

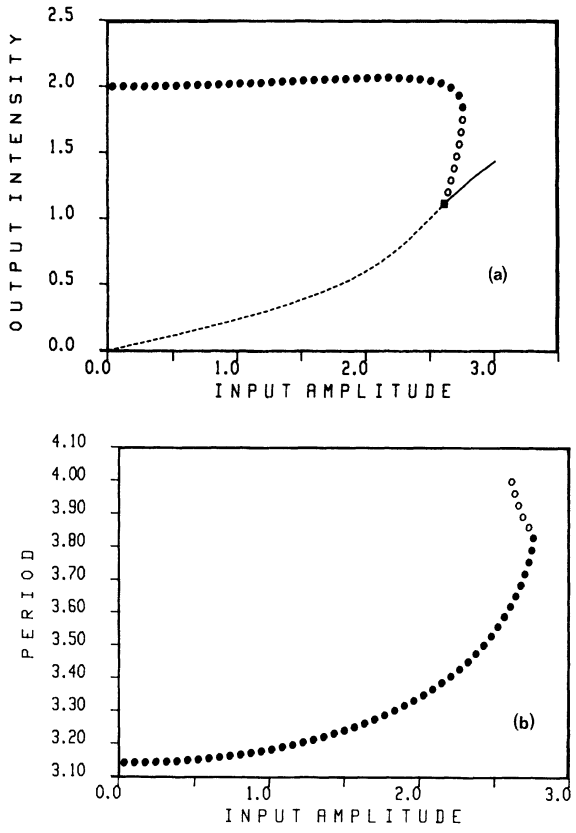

FIG. 6. Region II. (a) Bifurcation diagram with a subcritical HB. The open circles stand for the unstable periodic branch. (b) The period of the pulsating branch is given versus the bifurcation parameter.

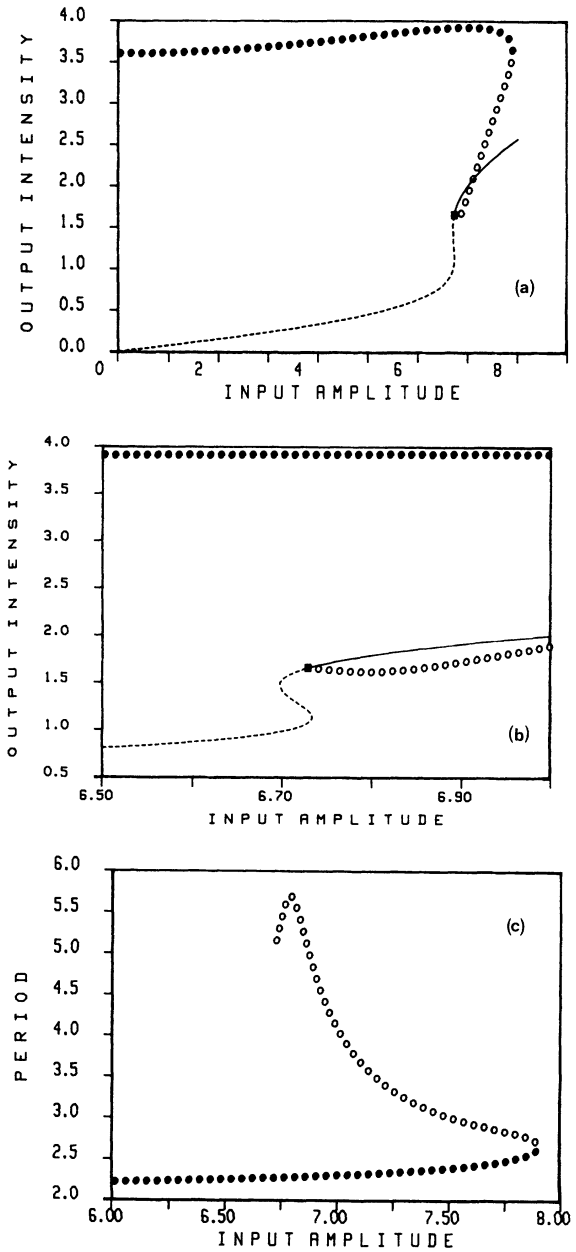

FIG. 7. Region IIIb. The subcritical HB is on the upper branch of the steady solutions. (a) Bifurcation diagram, (b) enlargement around the Hopf point, (c) period of the oscillating solution.

$\Omega=0.735$) describe these situations. The main difference between the two cases is that the Hopf periodic branch may join directly the lasing solution, "avoiding" the S-shape steady branch and more precisely the intermediate branch [Fig. 8(a)]. In that case one gets either bistability between two steady states or between a steady and a periodic solution. In Fig. 8(b) we display the period behavior which looks very similar to the one represented in Fig. 6(b). Nevertheless the maximum value reached by the period in the present case shows the effect of the homocline orbit proximity. The other possibility is that the Hopf branch cannot "avoid" that saddle-node steady branch and the two periodic branches of the problem are separated as displayed in Fig. 9(a): both of them finish their trajectory as homocline orbits, the normal branch on the upper steady turning point following the scheme which prevails in region I, while the Hopf branch separately bangs against the intermediate branch of steady states. This supports the interpretation of two different branches of periodic solutions, with two different origins introduced for the first time by Oppo *et al.* [12] through a frequency description on a three-dimensional model. These two branches can also merge following the observation of Ref. [13] on the absence of bifurcation at the junction point, and explained by the singular phase behavior of the two periodic solutions families.

For a comparison between the two- and three-dimensional models, we observe that the junction between the two periodic branches is a characteristic of the two-dimensional model (and approaching models: three dimensional but with small $\gamma_{\parallel}$ and very small detunings) while the bistability between the two branches needs a full three-dimensional model to occur. The presence of the homocline orbit seems to be common to all the models, even if in Ref. [12] they observe a decreasing frequency of the lasing branch but do not follow that branch far enough to conclude.

One can also deduce the continuous passage through region IIIa from the diagram of Fig. 4(a), governing below the lower boundary of that region and where we have only the "laser" branch, to the diagram of Fig. 5(a), valid above the upper boundary of region IIIa and where the Hopf branch is present and merges in the laser branch. As the input frequency increases, the Hopf appears on the lower branch and very near to the lower turning point such that the situation described on Fig. 9(a) prevails. Then the Hopf bifurcation goes down along the lower branch, and the S shape of the steady curve dies down: these two combined effects give rise to the behavior displayed in Fig. 8(a). We suppose that the homocline orbit climbs up on the intermediate branch as we move towards region II. To reach this last region (II) and

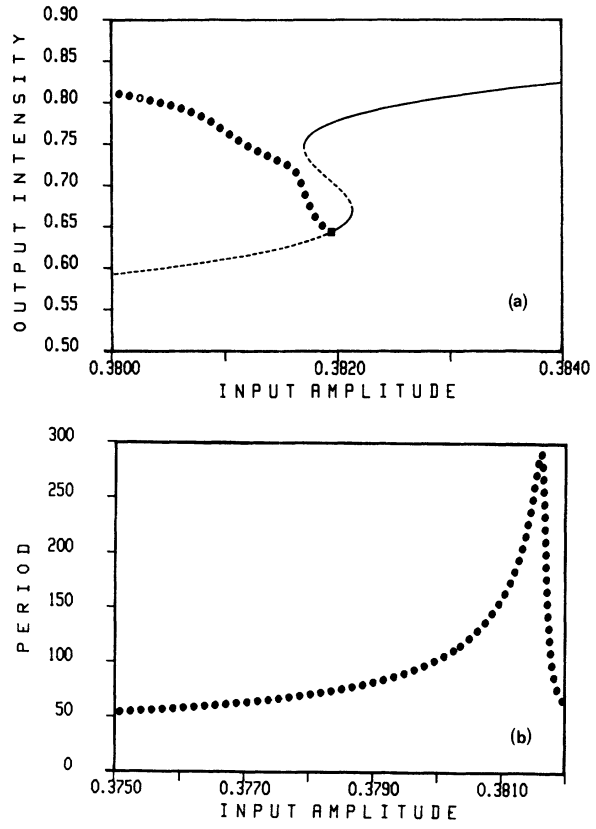

FIG. 8. Region IIIa. One of the system's evolution when the supercritical HB is present on the lower branch. (a) Bifurcation diagram for a "smooth" periodic branch; (b) evolution of the intensity period.

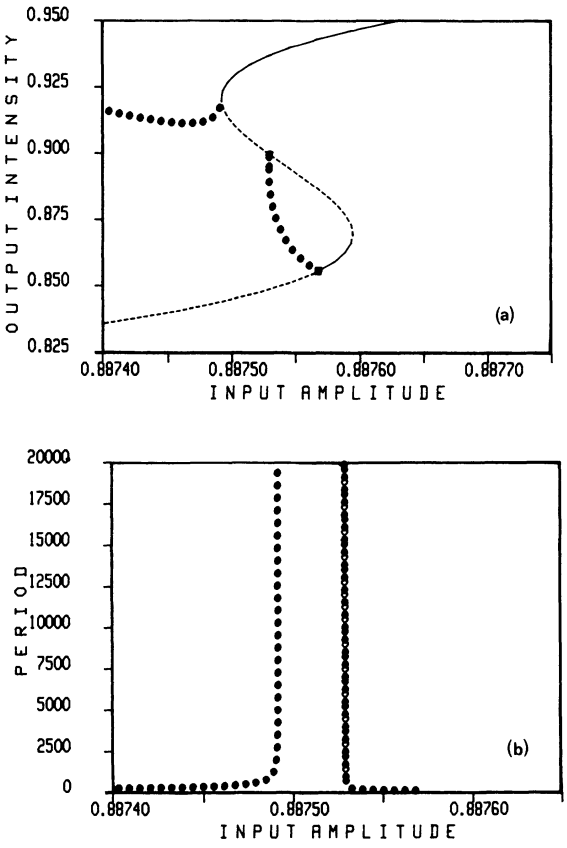

FIG. 9. Region IIIa. The second type of evolution of the system when the supercritical HB is present on the lower branch. (a) The presence of the homocline orbits break the periodic branch in two parts, (b) period of the pulsating branches.

the bifurcation diagram of Fig. 5(a), and as Ω increases one has just to notice that the intermediate branch progressively disappears. Figure 9(b) displays the separated periods of the two pulsating branches with the vertical asymptotic trajectory, signature of the homocline orbit presence. The same arguments may justify the continuity in the behavior description from region I to II through region IIIb.

Except the case described in Fig. 6 and the cases of a homocline orbit presence (region I and exceptionally IIIa), the period of the oscillating solutions shows in general an increase around the Hopf critical point and then a decrease towards the external signal period. In terms of frequencies, this represents a decrease followed by an increase towards the external frequency. These two kinds of behavior can be deduced from Eq. (31). Then the pushing frequency effect, which exists on the "normal" lasing branch (and then for small injections) and is described in Ref. [12] in the case of a three-dimensional model, is also present in this simplified model, but only on the Hopf periodic branch and close to the bifurcation point.

VII. CONCLUSIONS

We have used normal-form techniques to analyze the dynamics of the LIS. We have found a destabilization of the steady states via a Hopf bifurcation and demonstrated that the Hopf bifurcation can be localized on the upper or lower branch, but never on the intermediate branch. We have shown that it can be supercritical or subcritical and defined the parameter space accordingly. We have obtained the complete set of bifurcation diagrams the system may present and for any parametric situation. Our mathematical analysis complements previous investigations [12,13]. A continuous evolution in the parameter space connects the two-dimensional description to those of Refs. [13] and [12]. The reduction of the LIS model to the field equation only makes the system present a slightly different behavior: for example, no Hopf bifurcation on the intermediate branch, no bistability between the two periodic branches as computed in Ref. [12], and no frequency pushing of the periodic branches starting on the laser solution. However, all this information is underlying in the one-dimensional model: in region I, where no Hopf is present, the "critical" value $(\sqrt{R}-1)$ is always located on the intermediate branch; the two periodic branches are not bistable but they are still present in the system and they merge; finally, the frequency pushing occurs in some situations on the Hopf periodic branch close to the Hopf bifurcation point. The homocline orbit is also present in the one-dimensional system: this can be expected since we have the simultaneous presence of a saddle node and a limit cycle. Thus even though greatly simplified, which reduces the generality of the analysis to the so-called class-A lasers, the model we have analyzed shows some complicated behaviors. It offers also the advantage of fully developed analytical calculations.

Some of the complicated behaviors previously seen on the LIS, such as quasiperiodicity and chaotic attractors, however, disappear in such a two-dimensional description. One can expect to restore them by adding a modulation [20,21]. Since we know the behavior of the autonomous LIS for all parametric situations, the following paper [23] will be devoted to the dynamics of the modulated LIS.

ACKNOWLEDGMENTS

We wish to thank Professor P. Glorieux, Professor P. Mandel, and Professor Th. Erneux for very fruitful discussions and their encouragement. The authors are grateful to P. Van Ingelandt for his help to install the AUTO software on the CDC computer machine of the USTLI. The Laboratoire de Spectroscopie Hertzienne is "Unité de Recherche Associée du Centre National de la Recherche Scientifique."

APPENDIX A: CONSTRUCTION OF THE PERIODIC HOPF SOLUTIONS

In this appendix we give the main steps to solve Eq. (2) close to the Hopf point and by using the expansion (15). At the order zero, the perturbative method gives the definition of the Hopf point

$$\begin{aligned} &I_H u_H+\Omega v_H=-\mathcal{A}_H\ , \\ &\Omega u_H-I_H v_H=0\ , \end{aligned} \tag{A1}$$

while at first order in the linear problem of Eq. (16), the $2\otimes 2$ matrix $\underline{L}$ has the following elements:

$$\begin{aligned} &L_{uu}=I_H-2u_H^2,\quad L_{vv}=I_H-2v_H^2\ , \\ &L_{uv}=\Omega-2u_H v_H,\quad L_{vu}=-\Omega-2u_H v_H\ . \end{aligned} \tag{A2}$$

This linear problem has two eigenvalues $(\pm i\Omega_H)$ and related eigenvectors. X_1 is a linear combination of these eigenvectors as used in Eq. (17).

The ϵ^2 order leads to the fast-time evolution of u_2 and v_2 through the equation

$$\partial_t X_2=\underline{L}X_2+\underline{F}_2(t,\tau)\ , \tag{A3}$$

where the forcing term expression $\underline{F}_2(t,\tau)$ versus the problem parameters has the following components:

$$\begin{aligned} \underline{F}_{2u}=&a_2+u_1^2u_H\left\{-3+\frac{4u_H^2}{1+I_H}\right\}+v_1^2u_H\left\{-1+\frac{4v_H^2}{1+I_H}\right\} \\ &+2u_1v_1v_H\left\{-1+\frac{4u_H^2}{1+I_H}\right\}, \\ \underline{F}_{2v}=&u_1^2v_H\left\{-1+\frac{4u_H^2}{1+I_H}\right\}+v_1^2v_H\left\{-3+\frac{4v_H^2}{1+I_H}\right\} \\ &+2u_1v_1u_H\left\{-1+\frac{4v_H^2}{1+I_H}\right\}. \end{aligned} \tag{A4}$$

This term contains constant contributions (due to a_2 for example) and $\exp\{i\Omega_H t\},\exp\{2i\Omega_H t\}$ contributions provided from the products of the first-order solutions u_1 and v_1. The slow-time evolution is also present in the

$A(\tau)$ and $\beta(\tau)$ expressions which are still to be determined. The general solution of Eq. (A3) can be taken in the form:

$$X_2(t,\tau)=\begin{bmatrix}u_2(t,\tau)\\ v_2(t,\tau)\end{bmatrix} = \begin{bmatrix}\alpha_3(\tau)\\ \beta_3(\tau)\end{bmatrix}+\begin{bmatrix}\alpha_2(\tau)\\ \beta_2(\tau)\end{bmatrix}e^{i2\Omega_H t} + \begin{bmatrix}\alpha_1(\tau)\\ \beta_1(\tau)\end{bmatrix}e^{i\Omega_H t}+\text{c.c.}\ , \tag{A5}$$

where we note the presence of the harmonic contribution at the ϵ^2 order. Injecting Eq. (A5) in Eq. (A4), we get again a linear system for the complex α_i,β_i coefficients. We do not give their complete form because of their heaviness. We just note that $\beta_2(\tau)=Q\alpha_2(\tau)$, $\alpha_1(\tau)$, and $\beta_1(\tau)$ are functions of $A^2(\tau)$, while $\alpha_3(\tau)$ and $\beta_3(\tau)$ contain the time-independent term (a_2) and are proportional to $A(\tau)A^*(\tau)$.

The ϵ^3 order gives t-time evolution of u_3 and v_3, and a slow-time derivative ∂_τ appears. The vectorial equation can be expressed as

$$\partial_t X_3+\partial_t X_1=\underline{L}X_3+\underline{F}_3(t,\tau)\ , \tag{A6}$$

where the forcing term $\underline{F}_3$ has the following expressions:

$$\begin{aligned}
\underline{F}_{3u}=&v_1^2u_1\left\{-1+\frac{4I_H}{1+I_H}-24\frac{u_H^2v_H^2}{(1+I_H)^2}\right\}+u_1^2v_1\frac{12u_Hv_H}{1+I_H}\left\{1-\frac{2u_H^2}{1+I_H}\right\}\\
&+u_1^3\left\{-1+\frac{8u_H^2}{1+I_H}-\frac{8u_H^4}{(1+I_H)^2}\right\}+v_1^3\frac{4u_Hv_H}{1+I_H}\left\{1-\frac{2v_H^2}{1+I_H}\right\}\\
&+u_1u_2(2u_H)\left\{-3+\frac{4u_H^2}{1+I_H}\right\}+v_1v_2(2u_H)\left\{-1+\frac{4v_H^2}{1+I_H}\right\}\\
&+u_1v_2(2v_H)\left\{-1+\frac{4u_H^2}{1+I_H}\right\}+v_1u_2(2v_H)\left\{-1+\frac{4u_H^2}{1+I_H}\right\},\\
\underline{F}_{3v}=&u_1^2v_1\left\{-1+\frac{4I_H}{1+I_H}-24\frac{u_H^2v_H^2}{(1+I_H)^2}\right\}+v_1^2u_1\frac{12u_Hv_H}{1+I_H}\left\{1-\frac{2v_H^2}{1+I_H}\right\}\\
&+v_1^3\left\{-1+\frac{8v_H^2}{1+I_H}-\frac{8v_H^4}{(1+I_H)^2}\right\}+u_1^3\frac{4u_Hv_H}{1+I_H}\left\{1-\frac{2u_H^2}{1+I_H}\right\}\\
&+u_1u_2(2v_H)\left\{-1+\frac{4u_H^2}{1+I_H}\right\}+v_1v_2(2v_H)\left\{-3+\frac{4v_H^2}{1+I_H}\right\}\\
&+u_1v_2(2u_H)\left\{-1+\frac{4v_H^2}{1+I_H}\right\}+v_1u_2(2u_H)\left\{-1+\frac{4v_H^2}{1+I_H}\right\}.
\end{aligned} \tag{A7}$$

This term now presents secular terms (in $\exp\{i\Omega_H t\}$) which lead to an infinite contribution (with respect to the fast-time scale) for the X_3 solution. To get rid of them, we need a solvability condition. We write Eq. (A6) as

$$\partial t X_3=\underline{L}X_3-\partial_\tau X_1+\underline{F}_3(t,\tau)=\underline{L}X_3+C_{\text{inh}}(t,\tau) \tag{A8}$$

and the solvability condition takes the form

$$\int dt\{C_{\text{inh}}^{(1)u}\omega_3+C_{\text{inh}}^{(1)v}\nu_3\}=0\ . \tag{A9}$$

The integral occurs from 0 to $2\pi/\Omega$. The notation $C_{\text{inh}}^{(1)}$ stands for the inhomogeneous contributions and represents only the $\exp\{i\Omega_H t\}$ components of the $\underline{F}_3$ and $-\partial_\tau X_1$ terms. Note, however, that the inhomogeneous term can be fully considered since the other contributions vanish exactly. The Cartesian components ω_3 and ν_3 are those of the adjoint linear problem eigenvectors

$$\partial_t\mathcal{X}=\underline{M}\mathcal{X}\ , \tag{A10}$$

where $\underline{M}$ has the following matrix elements:

$$\begin{aligned}
&M_{uu}=I_H-2u_H^2,\quad M_{vv}=I_H-2v_H^2\ ,\\
&M_{uv}=-\Omega-2u_Hv_H,\quad M_{vu}=\Omega-2u_Hv_H\ .
\end{aligned} \tag{A11}$$

The solution $\mathcal{X}$ of the adjoint problem is

$$\mathcal{X}=\begin{bmatrix}\omega_3(t,\tau)\\ \nu_3(t,\tau)\end{bmatrix}=\begin{bmatrix}C(\tau)\\ D(\tau)\end{bmatrix}e^{i\Omega_H t}+\text{c.c.}\ , \tag{A12}$$

where $C=-Q^*D$ and Q is given in Eq. (18). Expanding Eq. (A9), one gets directly the normal form of Eq. (19) giving the slow-time evolution of the periodic-solution's complex amplitude appearing in the Hopf bifurcation surroundings.

APPENDIX B: PERIODIC BRANCH OF SOLUTIONS

In this appendix we present the direct integration of the equation system (26). The lowest order of the expansion (25) can be easily obtained since Eq. (26a) is fully integrable. In polar coordinates $x_0=\rho_0 e^{i\phi}$, one gets $\phi=-\Omega t+\phi_0$, and ρ_0 verifies the relation

$$(R-1-\rho_0^2)^{R/2}=K\rho_0\exp\{-(R-1)t\}\ , \tag{B1}$$

where K and ϕ_0 are constants depending on the initial conditions. In the long-time limit, $t\to\infty$, $\rho_0\to 0$ for $R<1$, and $\rho_0\to\sqrt{R-1}$ for $R>1$: this last limit is the well-known lasing solution. In terms of x_0 one can say that in the long-time limit and for $R>1$, $x_0\to\sqrt{R-1}e^{-i(\Omega t+\phi_0)}$ and we can drop the initial phase without loss of generality. If this asymptotic value of x_0 is valid, the ϵ-order equation also provides an integrable case that can be simplified if we lay down $u=x_1 e^{i\Omega t}$,

$$\frac{du}{dt}=-\frac{k}{2}(u+u^*)+ae^{i\Omega t}\ , \tag{B2}$$

where $k=2(R-1)/R$. Integrating this last equation, and going back to the previous variable x_1, we derive for the ϵ order of our expansion

$$x_1=e^{-i\Omega t}\left[c_2e^{-kt}+\frac{a}{k^2+\Omega^2}\{k\cos(\Omega t)+\Omega\sin(\Omega t)\}+i\left\{c_1-\frac{a}{\Omega}\cos(\Omega t)\right\}\right]\ . \tag{B3}$$

The c_2 term takes the form $-ak/(k^2+\Omega^2)$ and does not contribute for an infinite time, while the c_1 has to be zero valued to avoid secular influence on ϵ^2 order. We then get Eq. (27) of the paper. One can also write this last equation following the amplitude and phase expansions:

$$X(t)=[\sqrt{R-1}+\epsilon\rho_1(t)]e^{-i(\Omega t+\epsilon\psi_1)}\ , \tag{B4}$$

where

$$\rho_1(t)=\frac{a}{k^2+\Omega^2}\{k\cos(\Omega t)+\Omega\sin(\Omega t)\} \tag{B5}$$

and

$$\psi_1(t)=\frac{a}{\Omega\sqrt{R-1}}\cos(\Omega t)\ . \tag{B6}$$

These are the ϵth-order solutions of the Lindstedt-Poincaré expansion. The benefit of such an expansion is that it gives the ϵ^2-order phase or more precisely the frequency shift

$$\omega_2=-\frac{a^2}{R-1}\frac{\Omega}{k^2+\Omega^2}\ , \tag{B7}$$

which means that the laser frequency takes the value $\Omega_L=-\Omega-\epsilon^2\omega_2$. This expression signs a pulling to the external frequency as shown in Ref. [12].

[1] L. A. Lugiato, L. M. Narducci, D. K. Bandy, and C. A. Pennise, Opt. Commun. **46**, 64 (1983).
[2] Y. Gu, D. K. Bandy, J. M. Yuan, and L. M. Narducci, Phys. Rev. A **31**, 354 (1985).
[3] D. K. Bandy, L. M. Narducci, and L. A. Lugiato, J. Opt. Soc. Am. B **2**, 148 (1985).
[4] L. M. Narducci, J. R. Tredicce, L. A. Lugiato, N. B. Abraham, and D. K. Bandy, Phys. Rev. A **32**, 1588 (1985).
[5] D. K. Bandy, L. A. Lugiato, and L. M. Narducci, *Instabilities and Chaos in Quantum Optics,* edited by F. T. Arecchi and R. G. Harrison (Springer-Verlag, Berlin, 1987).
[6] Hu Gang and Yang Guo-jian, Phys. Rev. A **38**, 1979 (1988).
[7] D. J. Jones and D. K. Bandy, J. Opt. Soc. Am. B **7**, 2119 (1990).
[8] F. T. Arecchi, G. L. Lippi, G. P. Puccioni, and J. R. Tredicce, Opt. Commun. **51**, 308 (1984).
[9] F. T. Arecchi, G. L. Lippi, G. P. Puccioni, and J. R. Tredicce, in *Coherence and Quantum Optics V,* edited by L. Mandel and E. Wolf (Plenum, New York, 1984), p. 1227.
[10] G. L. Oppo and A. Politi, Z. Phys. B **59**, 111 (1985).
[11] J. R. Tredicce, F. T. Arecchi, G. L. Lippi, and G. P. Puccioni, J. Opt. Soc. Am. B **2**, 173 (1985).
[12] G. L. Oppo, A. Politi, G. L. Lippi, and F. T. Arecchi, Phys. Rev. A **34**, 4000 (1986).
[13] P. A. Braza and Th. Erneux, Phys. Rev. A **41**, 6470 (1990).
[14] A. Politi, G. L. Oppo, and R. Badii, Phys. Rev. A **33**, 4055 (1986).
[15] Hu Gang and Yang Guo-jian, Phys. Rev. A **40**, 834 (1989).
[16] R. Holzner, B. Derighetti, M. Ravani, and E. Brun, Phys. Rev. A **36**, 1280 (1987).
[17] A. Baugher, P. Hammack, and J. Lin, Phys. Rev. A **39**, 1549 (1989).
[18] P. A. Braza and Th. Erneux, Phys. Rev. A **40**, 2539 (1989).
[19] M. B. Spencer and W. E. Lamb, Jr., Phys. Rev. A **5**, 884 (1972).
[20] T. Yamada and R. Graham, Phys. Lett. **82A**, 321 (1981).
[21] H. J. Scholtz, T. Yamada, H. Brand, and R. Graham, Phys. Rev. Lett. **45**, 1322 (1980).
[22] G. V. Krivoshchekov, V. K. Makukha, V. M. Semibalamut, and V. S. Smirnov, Kvant. Elektron. (Moscow) **3**, 1782 (1976) [Sov. J. Quantum Electron. **6**, 965 (1976)].
[23] V. Zehnlé and H. Zeghlache, following paper, Phys. Rev. A **46**, 6030 (1992).
[24] G. Iooss and D. D. Joseph, *Elementary Stability and Bifurcation Theory* (Springer-Verlag, Berlin, 1980).
[25] P. Mandel, P. Galatola, L. A. Lugiato, and Wang Kaige, Opt. Commun. **80**, 262 (1990).
[26] P. Mandel, N. P. Pettiaux, Wang Kaige, P. Galatola, and L. A. Lugiato, Phys. Rev. A **43**, 424 (1991).
[27] H. Zeghlache, P. Mandel, N. B. Abraham, and C. O. Weiss, Phys. Rev. A **38**, 3128 (1988).
[28] E. Doedel, computer software AUTO, 1986.
[29] L. A. Lugiato, R. J. Horowicz, G. Strini, and L. M. Narducci, Phys. Rev. A **30**, 1366 (1984).